nature nanotechnology

SUPPLEMENTARY INFORMATION

DOI: 10.1038/NNANO.2013.267

Spin-resolved Andreev levels and parity crossings in hybrid superconductor-semiconductor nanostructures

Eduardo J. H. Lee, Xiaocheng Jiang, Manuel Houzet, Ramón Aguado, Charles M. Lieber, and Silvano De Franceschi

I. MODEL AND HARTREE-FOCK THEORY

As described in the main text, our nanowires are well described by a single-level quantum dot with competing superconducting correlations and on-site Coulomb interactions. A minimal model for describing this experimental configuration is given by a single level Anderson model coupled to a superconducting reservoir with Hamiltonian $H_{QD-S} = H_S + H_T^S + H_{QD}$. Here, H_{QD} models the uncoupled quantum dot, and is given by

$$H_{QD} = \sum_{\sigma=\uparrow,\downarrow} \epsilon_\sigma d_\sigma^\dagger d_\sigma + U n_\uparrow n_\downarrow, \tag{1}$$

where $d_\sigma^\dagger$ creates an electron with spin σ on the dot level located at ϵ_σ. In the presence of an external magnetic field B, spin-degeneracy is broken and the levels are given by $\epsilon_\uparrow = \epsilon_0 - \frac{1}{2}E_Z$ and $\epsilon_\downarrow = \epsilon_0 + \frac{1}{2}E_Z$ with $E_Z = g\mu_B B$, being the Zeeman energy. The second term in Eq. (1) describes the local Coulomb interaction for two electrons with opposite spin within the dot ($n_\sigma = d_\sigma^\dagger c_\sigma$), where U is the charging energy. H_S describes the uncoupled superconducting lead, modelled by a BCS Hamiltonian

$$H_S = \sum_{k_S\sigma} \xi_{k_S} c_{k_S\sigma}^\dagger c_{k_S\sigma} + \sum_{k_S} \left(\Delta c_{k_S\uparrow}^\dagger c_{-k_S\downarrow}^\dagger + \text{h.c.} \right), \tag{2}$$

where $\xi_{k_S} = \epsilon_{k_S} - \mu_S$ is referred with respect to the chemical potential at the superconducting reservoir μ_S and Δ is the superconducting order parameter. H_T^S describes the coupling between the QD level and the superconductor and has the form

$$H_T^S = \sum_{k_S\sigma} \left(V_{k_S} c_{k_S\sigma}^\dagger d_\sigma + \text{h.c.} \right).$$

This coupling to the superconducting lead is characterized by the parameter $\Gamma_S = \pi \sum_{k_S} |V_{k_S}|^2 \delta(\omega - \epsilon_{k_S})$. As described in the main text, the competition between the three energy scales U, Δ and Γ_S governs the ground state of the model which can be either a singlet or a doublet. Finally, the experimental setup includes a normal reservoir. We model this by adding two extra terms to the Hamiltonian such that the total model reads $H = H_N + H_T^N + H_{QD-S}$. The first term describes the normal reservoir and reads $H_N = \sum_{k_N,\sigma} \xi_{k_N} c_{k_N\sigma}^\dagger c_{k_N\sigma}$, where $c_{k_N\sigma}^\dagger$ creates an electron with spin σ at the single-particle energy level $\xi_{k_N} = \epsilon_{k_N} - \mu_N$, with μ_N being the chemical potential at the normal reservoir. The coupling to the normal lead is given by the term

$$H_T^N = \sum_{k_N\sigma} \left(V_{k_N} c_{k_N\sigma}^\dagger d_\sigma + \text{h.c.} \right),$$

which defines $\Gamma_N = \pi \sum_{k_N} |V_{k_N}|^2 \delta(\omega - \epsilon_{k_N})$.

All the relevant quantities for the experiment can be extracted from the QD Green's functions in Nambu space defined as $\hat{G}_\sigma^r(t,t') = -i\theta(t-t')\langle \left[\Psi_\sigma(t), \Psi_\sigma^\dagger(t')\right]_+ \rangle$, where $\Psi_\sigma = (d_\sigma \; d_{-\sigma}^\dagger)^T$. In frequency space, the QD Green's function can be formally written as $\hat{G}_\sigma^r(\omega)^{-1} = \hat{G}^{r,(0)}(\omega)^{-1} - \hat{\Sigma}_\sigma(\omega)$, where $\hat{G}^{r,(0)}(\omega)$ is the non-interacting dot Green's function in Nambu space and the self-energy $\hat{\Sigma}_\sigma$ takes into account both the coupling to the leads and the Coulomb interaction. Of course, the full problem cannot be exactly solved and one needs to resort to approximations. Here, we present calculations using a Hartree-Fock (HF) decoupling of the self-energy [1]. It has been demonstrated that such HF decoupling gives reliable results when benchmarked against more sophisticated methods such as numerical renormalization group [2]. We have opted for the HF treatment as it is able to provide a good qualitative description of the problem while being able to tackle with the cases of finite magnetic field and finite voltage. In analogy to other mean-field approaches, however, it does not capture Kondo correlations which become progressively more important with increasing Γ_S. Nevertheless, the qualitative description of the competition between singlet and doublet states is not affected, as the main role of the Kondo effect is to reduce the extension of the doublet region in the phase diagram [3, 4].

DOI: 10.1038/NNANO.2013.267

The HF selfenergy is obtained by considering the first order diagrams in the Coulomb interaction. Its diagonal components in Nambu space are given by $\Sigma^{HF}_{11,\sigma} = -\Sigma^{HF}_{22,-\sigma} = U\langle n_{-\sigma}\rangle$, where the spin-resolved occupations $\langle n_\sigma\rangle = -\frac{1}{\pi}\int d\omega Im G^r_{11,\sigma}(\omega)$ have to be calculated *self-consistently*. Importantly, also the anomalous self-energies $\Sigma^{HF}_{12,\sigma} = (\Sigma^{HF}_{21,\sigma})^* = -U\langle d_\uparrow d_\downarrow\rangle$ have to be taken into account. The explicit expression for $\hat{G}^{r,HF}_\sigma(\omega)$ reads

$$\hat{G}^{r,HF}_\sigma(\omega) = \frac{1}{D(\omega)}\begin{pmatrix} \omega+\epsilon_{-\sigma}+i\Gamma_N+\Gamma_S\frac{\omega}{\sqrt{\Delta^2-\omega^2}}+U\langle n_\sigma\rangle & \Gamma_S\frac{\Delta}{\sqrt{\Delta^2-\omega^2}}+U\langle d_\uparrow d_\downarrow\rangle \\ \Gamma_S\frac{\Delta}{\sqrt{\Delta^2-\omega^2}}+U\langle d^\dagger_\downarrow d^\dagger_\uparrow\rangle & \omega-\epsilon_\sigma+i\Gamma_N+\Gamma_S\frac{\omega}{\sqrt{\Delta^2-\omega^2}}-U\langle n_{-\sigma}\rangle \end{pmatrix}. \quad (3)$$

The Andreev level spectrum of the system is given by the roots of the determinant $D(\omega) \equiv Det[\hat{G}^{r,HF}_\sigma(\omega)^{-1}]$, namely by the solutions of

$$\begin{aligned}(\omega-\epsilon_\sigma+i\Gamma_N+\Gamma_S\frac{\omega}{\sqrt{\Delta^2-\omega^2}}-U\langle n_{-\sigma}\rangle)(\omega+\epsilon_{-\sigma}+i\Gamma_N+\Gamma_S\frac{\omega}{\sqrt{\Delta^2-\omega^2}}+U\langle n_\sigma\rangle)\\ -(\Gamma_S\frac{\Delta}{\sqrt{\Delta^2-\omega^2}}+U\langle d_\uparrow d_\downarrow\rangle)(\Gamma_S\frac{\Delta}{\sqrt{\Delta^2-\omega^2}}+U\langle d^\dagger_\downarrow d^\dagger_\uparrow\rangle)=0. \quad (4)\end{aligned}$$

The QD spectral function is defined as $A(\omega) = -\frac{1}{\pi}ImTr[\hat{G}^{r,HF}_\sigma(\omega)]$, where the trace includes both spin and Nambu degrees of freedom.

In practice, the results presented below were obtained by discretizing the Fourier space in a finite mesh of size $N = 2^{18}$ with $\omega_i \in [-D, D]$ and cutoff $D = 25\Delta$. Starting from an initial effective mean-field solution $\Sigma_{11,\uparrow} = -\Sigma_{22,\downarrow} = \frac{U}{2}$ [5], we iterate the HF equations until good numerical convergence in the spin-resolved occupations is reached (as a criterium for good convergence, the iteration stops when the relative error between successive occupations in the iteration loop is less than 10^{-5}).

For a given bias voltage $eV = \mu_N - \mu_S$, the conductance across the system is given by $\mathcal{G} = dI/dV$, where the total current can be decomposed into Andreev and quasiparticle contributions, $I = I_A + I_Q$. For voltages $eV \leq \Delta$, the quasiparticle current is zero, $I_Q = 0$, and the only contribution comes from Andreev processes. The Andreev current reads

$$I_A = \frac{2e}{h}\int d\omega[f_N(\omega - V) - f_N(\omega + V)]T_A(\omega), \quad (5)$$

where the Andreev transmission, defined as

$$T_A(\omega) = 4\Gamma_N^2\sum_\sigma |G^{HF}_{12,\sigma}(\omega)|^2, \quad (6)$$

describes processes in which an electron (hole) from the normal side is reflected as a hole (electron) while an extra Cooper pair is created on the superconducting side. For voltages above the gap, also the quasiparticle contribution is finite and is given by:

$$I_Q = \frac{2e}{h}\int d\omega[f_N(\omega - V) - f_S(\omega)]T_Q(\omega), \quad (7)$$

with a quasiparticle transmission defined as

$$T_Q(\omega) = 4\Gamma_N\Gamma_S\theta(|\omega|-\Delta)\frac{|\omega|}{\sqrt{\omega^2-\Delta^2}}\sum_\sigma[|G^{HF}_{11,\sigma}(\omega)|^2 + |G^{HF}_{12,\sigma}(\omega)|^2 - \frac{2\Delta}{|\omega|}Re\{G^{HF}_{11,\sigma}(\omega)[G^{HF}_{12,\sigma}(\omega)]^*\}]. \quad (8)$$

This quasiparticle contribution consists of three proccesses: 1) conventional tunneling, 2) an electron (hole) in the normal side is converted into a hole (electron) excitation in the superconducting side (branch crossing [6]), and 3) quasiparticle transfer from the normal lead into the superconducting lead, while creating (or annihilating) a Cooper pair as an intermediate state.

In Fig. S1 we show the resulting theoretical dI/dV plots. The full phenomenology discussed in the main text, *i.e.*, (i) the doublet to singlet transition with increasing Γ_S ($B = 0$), (ii) the B-field dependence of Andreev levels, namely their splitting or shift to higher energies depending whether the system is in a singlet or doublet ground state (GS), respectively, and (iii) the field-induced quantum phase transition from a singlet GS to a spin-polarized GS (see middle column), is recovered. In the calculations, we have adjusted the device parameters in order to get the best qualitative agreement between the theory plots and the experimental data shown in Fig. 2 of the main text

($U = 2.5\Delta$, $\Gamma_S/\Gamma_N = 3$, and $\Gamma_S = 0.2\Delta$, 0.7Δ and 0.9Δ). We note that in the simulations, the tunnel coupling to the normal contact, Γ_N, was deliberately enhanced, thereby substantially decreasing the tunnel coupling asymmetry when compared to the experimental value $\Gamma_S/\Gamma_N \approx 100$. By doing this, the numerical convergence of the calculations is significantly improved, especially in proximity of abrupt crossings in the ground state parity [2]. At the same time, the underlying physical picture is not affected, as in our model, Γ_N only impacts the broadening of Andreev levels. The good qualitative agreement between theory and experiment strongly supports our interpretation in terms of spin-resolved Andreev levels and a quantum phase transition.

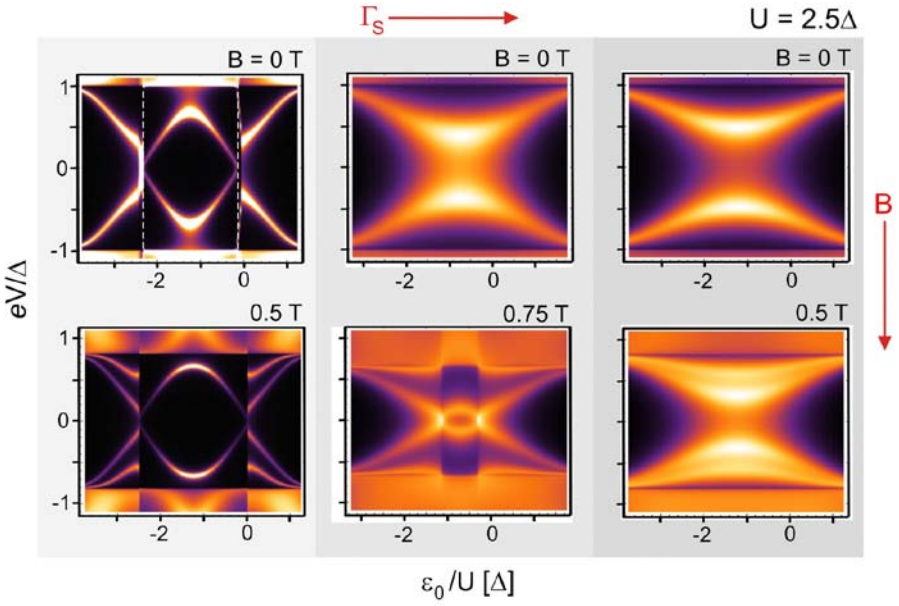

Fig. S 1: Theoretical dI/dV plots calculated by means of a self-consistent Hartree-Fock theory. In all calculations we used $U = 2.5\Delta$ and $\Gamma_S/\Gamma_N = 1/3$. From left to right, Γ_S was set to 0.2Δ, 0.7Δ and 0.9Δ. The bottom row depicts the effect of an external magnetic field on the sub-gap Andreev levels. Despite the relative simplicity of the Anderson model, the full experimental phenomenology is recovered.

Fig. S2 displays the calculated B-dependences of Andreev levels for the cases in which the QD-S system is initially in a doublet (left panel) or singlet (right panel) GS. Once again, the theory plots show good qualitative agreement with the experimental data (Fig. 3 of main text). Importantly, the experimentally observed pinning of the QPT peak at zero-bias, resulting from the energy level repulsion effect in combination with the closing of the superconducting gap (Fig. 3c, main text) is reproduced by the numerical calculations (see right panel of Fig. S2).

II. ANALYTIC MODEL FOR ENERGY LEVEL REPULSION

Below we derive a simple expression which describes the level repulsion between the doublet states and the states in the continuum of the superconducting lead at small coupling $\Gamma_S \ll \Delta$, in the regions of gate voltage corresponding to a singlet ground state.

The Hamiltonian for the superconducting lead given by Eq. (2) can be diagonalized after a Bogoliubov transformation,

$$H_S = \sum_{k_S\sigma} \epsilon_{k_S} \gamma^\dagger_{k_S\sigma} \gamma_{k_S\sigma}, \tag{9}$$

where $\gamma_{k_S\sigma} = u_{k_S} c_{k_S\sigma} + \sigma v_{k_S} c^\dagger_{-k_S-\sigma}$ are the annihilation operators of Bogoliubov quasiparticles with energy $\epsilon_{k_S} = [\Delta^2 + \xi^2_{k_S}]^{1/2}$, and $u_{k_S}, v_{k_S} = [(1 \pm \xi_{k_S}/\epsilon_{k_S})/2]^{1/2}$ are the BCS coherence factors. The projection of the Hamiltonian H_{QD-S} to a subspace of states with energy close to Δ in the leads then reads

$$H_{QD-S} = \sum_{k_S\sigma} \left(\Delta + \frac{\xi^2_{k_S}}{2\Delta} \right) \gamma^\dagger_{k_S\sigma} \gamma_{k_S\sigma} + H_{QD} + \frac{1}{\sqrt{2}} \sum_{k_S} \left[V_{k_S} \left(\gamma^\dagger_{k_S\sigma} - \sigma \gamma_{k_S-\sigma} \right) d_\sigma + \text{h.c.} \right]. \tag{10}$$

DOI: 10.1038/NNANO.2013.267

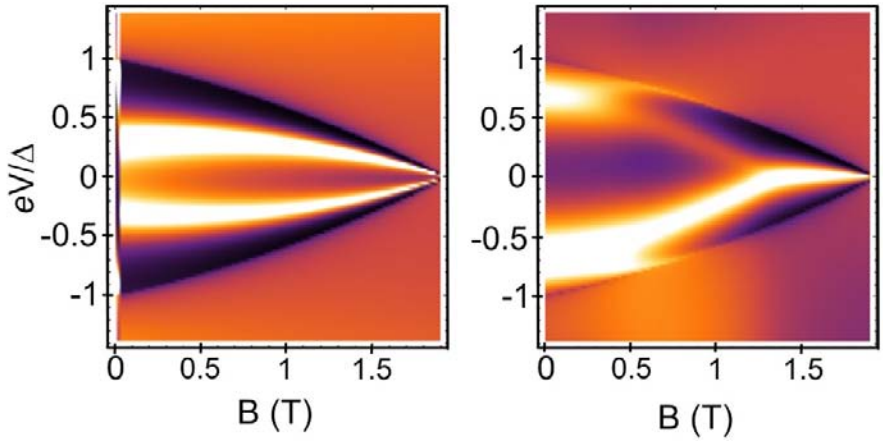

Fig. S 2: Theoretical $dI/dV(B, eV/\Delta)$ plots using the parameters $U/\Delta = 8$, $\epsilon_0/\Delta = -4$ and $\Gamma_S/\Delta = 1.5$ (Γ_N/Γ_S was set to 1/3). The left (right) depicts the B-dependence of Andreev levels when the QD-S system is in the singlet (doublet) ground state.

The sums in the r.h.s of this equation are restricted to momenta such that $|\xi_{k_S}| \ll \Delta$, and $u_{k_S}, v_{k_S} \approx 1/\sqrt{2}$.

At vanishing tunnel coupling, the ground state at $\epsilon_\uparrow > 0$ is the product state of the BCS ground state in the lead and the empty level in the dot, which we denote $|\emptyset\rangle$. Lowest energy excited states consist of the singly occupied level, $d^\dagger_\sigma|\emptyset\rangle$, as well as the BCS ground state filled with one Bogoliubov quasiparticle, $\gamma^\dagger_{k_S\sigma}|\emptyset\rangle$. When their energies ϵ_σ and ϵ_{k_S} are close and the tunnel couplings V_{k_S} are finite, the discrete state on the dot and the continuum of states in the leads hybridize. Then, we may use $|\Psi_\sigma\rangle = (Ad^\dagger_\sigma + \sum_{k_S} B_{k_S}\gamma^\dagger_{k_S\sigma})|\emptyset\rangle$ as a variational wavefunction for the excited states with spin σ. From the set of equations

$$(E - \epsilon_\sigma)\, A \;=\; \frac{1}{\sqrt{2}} \sum_{k_S} V^*_{k_S} B_{k_S}, \tag{11a}$$

$$\left(E - \Delta - \frac{\xi^2_{k_S}}{2\Delta}\right) B_{k_S} \;=\; \frac{1}{\sqrt{2}} V_{k_S} A, \tag{11b}$$

that determine possible eigenenergies E associated with the wavefunction $|\Psi_\sigma\rangle$, we obtain the following equation for the bound state excitation energy $\zeta_\sigma \approx E$ of state $|\sigma\rangle$:

$$\zeta_\sigma - \epsilon_\sigma = -\Gamma_S \sqrt{\Delta/[2(\Delta - \zeta_\sigma)]}. \tag{12}$$

It yields

$$\zeta_\sigma \simeq \begin{cases} \epsilon_\sigma - \Gamma_S\sqrt{\Delta/[2(\Delta-\epsilon_\sigma)]}, & \Delta - \epsilon_\sigma \gg (\Gamma_S^2\Delta)^{1/3}, \\ \Delta - (\Gamma_S^2\Delta/2)^{1/3}, & \epsilon_\sigma \simeq \Delta, \\ \Delta - \Gamma_S^2\Delta/[2(\epsilon_\sigma - \Delta)^2], & \epsilon_\sigma - \Delta \gg (\Gamma_S^2\Delta)^{1/3}. \end{cases} \tag{13}$$

Equation (13) describes the anticrossing (or level repulsion) between the dot state and the BCS continuum. Namely, a bound state forms at all values of ϵ_σ; it gets closer to the edge of the BCS continuum – and the splitting $|\zeta_\downarrow - \zeta_\uparrow|$ vanishes – as ϵ_σ is increased. Note that the excitation energy of the bound state coincides with the Andreev level energy obtained from Eq. (4) at $\Gamma_S \ll \Delta$, in the regions near the edge of the continuum spectrum in the lead, where $\langle n_\uparrow\rangle = \langle n_\downarrow\rangle = 0$ and the last term in the l.h.s gives a negligible correction in $(\Gamma_S/\Delta)^{2/3} \ll 1$.

Similarly, when $\epsilon_{-\sigma}$ is close to $-(U + \Delta)$, and the dot is doubly occupied in the ground state $d^\dagger_\uparrow d^\dagger_\downarrow|\emptyset\rangle$ at vanishing tunnel coupling, we may use $|\Psi_\sigma\rangle = (Ad^\dagger_\sigma + \sum_{k_S} B_{k_S}\gamma^\dagger_{k_S\sigma} d^\dagger_\uparrow d^\dagger_\downarrow)|\emptyset\rangle$ as a variational wavefunction at finite coupling and obtain the equation

$$\zeta_\sigma + \epsilon_{-\sigma} + U = -\Gamma_S\sqrt{\Delta/[2(\Delta - \zeta_\sigma)]}. \tag{14}$$

for $\zeta_\sigma \approx E - (2\epsilon + U)$. It is also in correspondence with Eq. (4) in the regions where $\langle n_\uparrow\rangle = \langle n_\downarrow\rangle = 1$.

III. MAGNETIC FIELD DEPENDENCE OF Δ

The magnetic field dependence of the superconducting gap, Δ, was estimated from the dI/dV vs (B,V) measurement shown in Fig. S3a, which was taken at the center of an even valley. As discussed in the main text, the Andreev levels appear at $eV \pm \Delta$ when the system lies deep inside the singlet GS. Thus, $\Delta(B)$ is readily obtained from the evolution of the sub-gap resonances as a function of B (Fig. S3b). This experimental dependence was used for obtaining the theoretical dI/dV plots at finite B (shown in Figs. 2 and 3 of the main text).

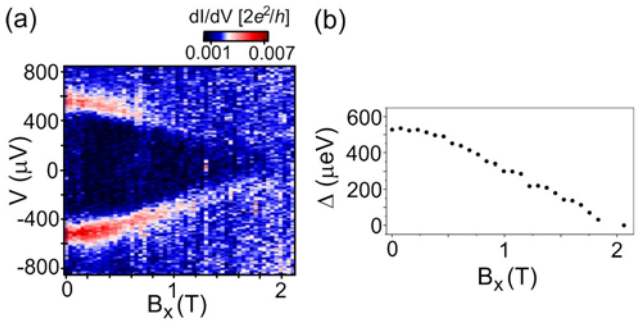

Fig. S 3: (a) dI/dV vs. (B,V) measurement taken at the center of an even valley. (b) Superconducting gap extracted from (a) as a function of B_x.

IV. CHARACTERIZATION OF SECOND S-QD-N DEVICE

Here we present additional data obtained from the device discussed in Figs. 3 and 4 of the main text. The device was first characterized in the normal state (Fig. S4a). To this end, an external magnetic field $B = 2.5$ T was applied above the critical field $B_c \approx 2$ T, driving the vanadium electrical leads across the superconducting transition. The resulting charge stability diagram revealed a split Kondo resonance within the odd-occupied diamond (highlighted by the white arrows). Furthermore, a charging energy $U \approx 4.5$ meV is extracted from the height of the Coulomb diamond, whereas an average tunnel coupling $< \Gamma > \approx 0.8$ meV is estimated from the FWHM of the Coulomb resonances.

The series of dI/dV vs. (V_{pg},V) plots shown in Fig. S4b ($B = 0$, 0.5 and 0.75 T) depicts the B-field evolution of the sub-gap Andreev levels in the second device. It is noteworthy that the data herein discussed shows a shift of ≈ 20 meV in the V_{pg} axis when compared to the corresponding plot in the main text (Fig. 3a). This can be attributed to a local charge rearrangement in the vicinity of the QD which, due to capacitive coupling, effectively results in a small shift of the charge stability diagram. In spite of the shift, the dI/dV features clearly remain unaltered. The data shown in Fig. S4 is qualitatively analogous to the situation discussed in the top (experimental) row of Fig. 2 in the main text. Specifically, at $B = 0$ (left-most panel), the sub-gap resonances cross twice the Fermi level, delimiting the boundaries between the singlet (S) and doublet (D) ground states (GSs). In agreement with the discussion in the manuscript, the Andreev levels split with increasing magnetic field when the system lies in the singlet GS.

V. SUPPLEMENTARY DATA ON ENERGY LEVEL REPULSION EFFECT

Fig. S5 contains further information concerning the energy level repulsion effect discussed in the manuscript. The right panel of Fig. S5a displays an additional dI/dV vs (B,V) measurement taken at the position of the dashed line in the left panel, which is further away from the crossing point than position 2 in Fig. 3a of the main text. As discussed in the manuscript, the B-dependence of the $\zeta_{\downarrow}$ peaks deviates from the expected Zeeman splitting of the doublet state, due to the level repulsion of the $|\downarrow>$ state by the continuum of quasiparticle states above the superconducting gap. Fig. S5b demonstrates that this effect becomes more pronounced as the energy of the $\zeta_{\downarrow}$ peaks approaches Δ, as expected from theory. The plotted g-factor values were estimated from the slopes of the $\zeta_{\uparrow,\downarrow}$ vs. B data (red circles and blue triangles, respectively). The horizontal dashed line is positioned at $g \approx 5.5$, corresponding to the value estimated from the inelastic cotunneling dI/dV steps in the normal state (shown in Fig. S5c). By its turn, the vertical dashed line signals the position of the singlet-doublet phase boundary. The plot clearly shows how

DOI: 10.1038/NNANO.2013.267

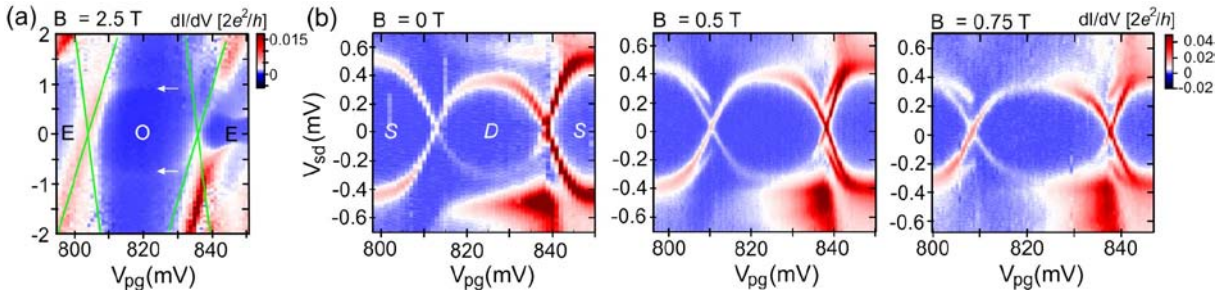

Fig. S 4: (a) Characterization of second device in the normal state ($B = 2.5$ T). The green lines are guides to the eye depicting the limits of the Coulomb diamonds with even (E) and odd (O) occupation. The white arrows highlight inelastic cotunneling steps in dI/dV related to the split Kondo resonance. (b) Effect of B on the Andreev levels observed in the same device. A series of dI/dV vs (V_{pg}, V) plots taken at $B = 0$, 0.5 and 0.75 T is shown. S and D indicate the regions in which the ground state is a singlet or a doublet, respectively.

the g-factor extracted from the $\zeta_\downarrow$ peaks is strongly suppressed when moving away from the crossing point. The values obtained from the $\zeta_\uparrow$ peaks, on the other hand, show no significant plunger gate dependence.

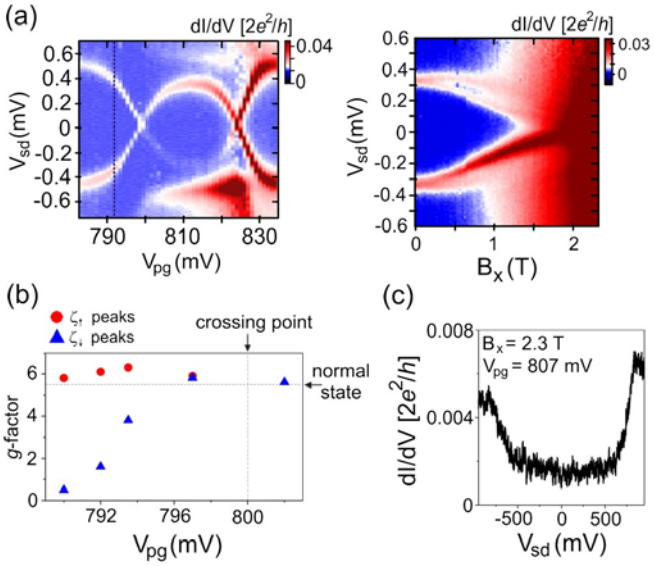

Fig. S 5: (a) Right panel: dI/dV vs. (B, V) plot taken at the position marked by the dashed line in the left panel. The measurement shown in the left panel is the same as that shown in Fig. 3a in the main text. (b) g-factor estimated from $\zeta_\uparrow$ and $\zeta_\downarrow$ peaks as a function of V_{pg}. The level repulsion effect is evidenced by the suppressed $\zeta_\downarrow$ g-factor at positions further away from the crossing point, where the $\zeta_\downarrow$ peak energy approaches Δ. (c) Inelastic cotunneling dI/dV steps resulting from the field-induced splitting of a spin-1/2 Kondo resonance. This measurement, taken at $B = 2.3$ T, yields a normal state $g \approx 5.5$.

VI. SUPPLEMENTARY DATA ON ANGULAR DEPENDENCE OF THE ANDREEV LEVELS AT FINITE B

To complement the angular dependence data shown in Fig. 4b of the main text, we include here the complete B-field dependences measured at $\theta = 0, \pi/2$ (Fig. S6a). The plot shown in the left panel ($\theta = 0$) is analogous to the measurement shown in Fig. 4a of the main text. From this, a QPT field $B^x_{QPT} \approx 0.6$ T is estimated. The corresponding QPT measurement at $\theta = \pi/2$ (right panel) shows the same qualitative features, however with two significant differences. The most relevant difference is that the slope of the Andreev levels is reduced, indicating a smaller g-factor. This results in a QPT field $B^y_{QPT} > 1$ T. The g-factor anisotropy is highlighted in Fig. S6b, where the data points were extracted from the angular dependence of $\zeta_\uparrow$ and $\zeta_\downarrow$ at a field magnitude $|B| = 0.6$ T (data shown in Fig. 4b of the main text). The second difference between the two data plots in Fig. S6a is in the value of

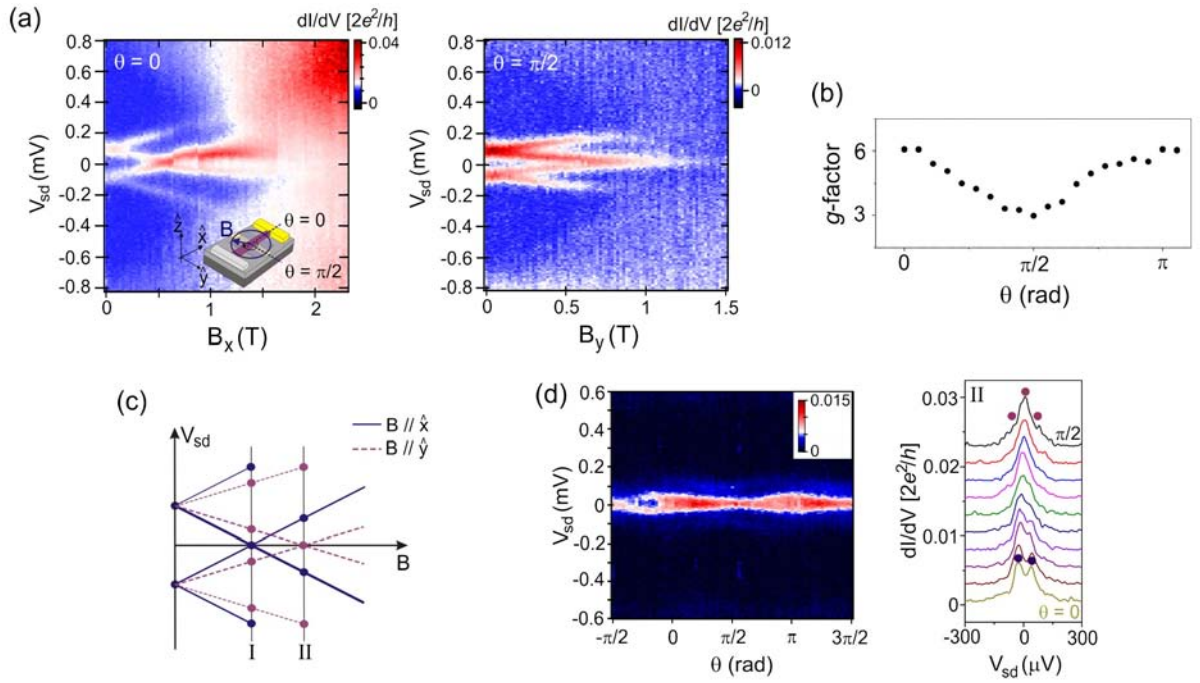

Fig. S 6: (a) B-field dependences of the Andreev levels measured at $\theta = 0$ (left panel) and $\theta = \pi/2$ (right panel). The inset in the left panel shows the orientation of the field with respect to the nanowire ($\theta = 0$ corresponds to B aligned parallel to NW). (b) g-factor anisotropy measured from the Andreev level splitting at $|B| = 0.6$ T. (c) Schematic diagram summarizing the angular dependence behaviour. Due to the g-factor anisotropy, the QPT occurs at different fields for $\theta = 0$ (solid blue line) and $\pi/2$ (dashed violet line). Lines I and II highlight the dI/dV features observed when $|B|$ is fixed at $|B^x_{QPT}|$ and $|B^y_{QPT}|$, respectively. (d) Angular dependence measurement taken with $|B| = |B^y_{QPT} = 0.35$ T. Here, the zero-bias QPT peak appears for B perpendicular to the nanowire axis. The circles in the line profile plot (right panel) ascribes the measured dI/dV peaks to the Andreev levels shown in (c).

the respective critical fields: $B^x_c \approx 2$T against $B^x_c \approx 1.5$T.

The scheme depicted in Fig. S6c summarizes the evolution of the Andreev levels for the longitudinal (solid line) and perpendicular (dashed line) field directions, as deduced from the data in panel (a). For a field amplitude $|B| = |B^x_{QPT}| = 0.6$ T, a zero-bias peak (ZBP) is observed at $\theta = 0$ (or $\theta = \pi$) in correspondence of the blue dot along line I. At $\theta = \pi/2$ (or $\theta = 3\pi/2$), the ZBP is split into two peaks in correspondence of the violet dots along line I. This is indeed the behaviour observed in Fig. 4b of the main text. The scenario is reversed when the field magnitude $|B|$ is fixed at $|B^y_{QPT}|$ (as indicated by line II). Unfortunately, the QPT in the perpendicular direction occurs near the closing of the gap (Fig. S6a). To better visualize the angular dependence of the Andreev levels in the case $|B| = B^y_{QPT}$, the V_{pg} position was moved closer to the singlet-doublet phase boundary, so that the Andreev levels are closer to the Fermi level at $B = 0$. Fig. S6d shows the angular dependence measurement taken at $|B| = 0.35$ T. In this case a ZBP is observed for $\theta = \pi/2$ (or $\theta = 3\pi/2$), in correspondence of the violet dot along line II, while a split peak is observed for $\theta = 0$ (or $\theta = \pi$), as denoted by the pair of blue dots along line II.

VII. RELEVANCE TO TUNNEL SPECTROSCOPY EXPERIMENTS AIMING AT THE OBSERVATION OF MAJORANA FERMIONS

Following recent theoretical proposals [7, 8], the past years have seen intense experimental efforts for the realization and detection of Majorana fermions (MFs) in hybrid superconductor-semiconductor nanowire devices. These exotic quasiparticles are predicted to arise in hybrid devices consisting of a semiconductor nanowire with strong spin-orbit coupling (*e.g.*, InSb, InAs) coupled to an s-wave superconductor, and in the presence of an external magnetic field, B, applied perpendicular to the Rashba spin-orbit field, B_{SO}. When the Zeeman energy, $E_Z = g\mu_B B$, exceeds the critical value $2\sqrt{\Delta^2_{ind} + \mu^2}$, where Δ_{ind} is the superconducting gap induced in the NW by the proximity effect and μ is the chemical potential, the NW section underneath the superconductor undergoes a transition into a topological superconducting phase, and zero-energy MF states are formed at its edges. So far, the experimental hunt for MFs

DOI: 10.1038/NNANO.2013.267

in hybrid devices has predominantly relied on dc transport experiments aiming at the detection of these zero-energy states through ZBPs in the differential conductance [9–13]. In this relatively simple approach, it is essential to understand and rule out all other physical effects that could give rise to ZBPs (*e.g.*, reflectionless tunneling [14], weak antilocalization [15], Kondo effect [16], etc.). Here we extend our discussion on the ZBPs resulting from Andreev levels crossing the Fermi energy under the action of an applied magnetic field. We show that this physical mechanism is particularly relevant since it can produce experimental signatures that can resemble very much those expected from MFs. We aim to highlight such signatures, make comparisons to existing experiments, and provide guidelines to distinguish ZBPs stemming from zero-energy Andreev levels from those due to MFs. Our work deals with QDs with on-site Coulomb repulsion, rather than non-interacting one-dimensional structures, which are required by the proposals on MFs. Yet we wish to emphasize that our conclusions may still hold relevance to existing experiments where, to our view, interactions cannot be ruled out with certainty (we note that the reported ZBPs have amplitudes below the conductance quantum, and that electron localization may arise even at the level of individual barriers formed by a local charge depletion of the nanowire).

ZBPs due to MFs are predicted to follow a characteristic magnetic-field dependence. In superconductor-nanowire devices, a MF ZBP is expected to emerge only for finite fields perpendicular to B_{SO} (due to symmetry arguments, this latter should lie most likely in the device plane perpendicular to the nanowire axis). Therefore, logically, the MF ZBP should disappear when a rotation brings the magnetic field parallel to B_{SO}. For field directions perpendicular to B_{SO}, the ZBP should be stable against further increases in the field magnitude, provided the nanowire is sufficiently long. In this case, the two MF modes located at the ends of the topological nanowire do not overlap, and consequently, remain at zero energy. By contrast, shorter nanowires are expected to display a sizable splitting of the ZBP due to the hybridization of the MF modes. It is predicted that this splitting should be modulated in an oscillatory fashion by variations in the magnitude of the magnetic field [17–19].

Let us now discuss to what extent the just mentioned fingerprints of MF ZBPs can be found in Andreev-level ZBPs.

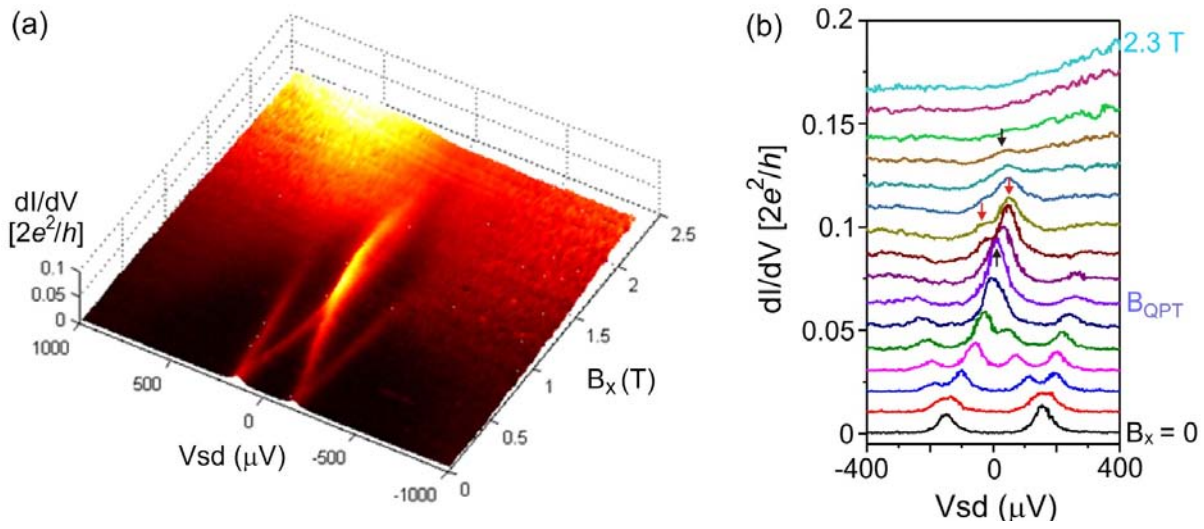

Fig. S 7: (a) $dI/dV(B_x, V)$ taken at a position slightly further from the singlet-doublet crossing as that shown in Fig. 4a (main text). As a result, the QPT ZBP appears at a larger magnetic field ($B_x^{QPT} \approx 0.9$ T). (b) $dI/dV(V)$ line profiles of the dataset shown in (a). With increasing field, a black arrow first highlights the QPT ZBP ($B = B_{QPT}$). A second black arrow indicates another ZBP which results from the "squeezing" of ζ peaks (marked by red arrows) with the closing of the gap. This re-emergence of the ZBP with increasing field qualitatively mimics the oscillatory hybridization of MFs.

A. Emergence of Andreev-level ZBPs at finite field and their stability against B variations.

As shown in Fig. 4 (main text), the observed ZBP persists over a field range $\Delta B_x \approx 150$ mT. This range is consistent with that expected from the finite width w of the Andreev level crossing the Fermi energy, i.e. $\Delta B \approx w/(|g|\mu_B)$. Interestingly, the ZBP reported by Das *et al.* [10] (hybrid devices based on InAs NWs coupled to Al superconducting electrodes), displays features qualitatively very similar to those of Fig. 4 (main text). To emphasize this similarity we show in Fig. S5a a data set of the same type plotted on a three-dimensional color scale similar to the one of Fig. 4a in ref. 10. Thus, let us discuss how far an Andreev-level picture can be fitted to the experimental results of ref. 10.

In Fig. 4a of ref. 10, two dI/dV peaks at $V_{sd} = \pm 45$ μeV are observed at zero magnetic field. These peaks are interpreted as the edges of the induced superconducting gap, Δ_{ind}. The fact that the two peaks approach each other as a result of an applied magnetic field is interpreted as the closure of this gap. Here we consider a different scenario where the two peaks (at $B = 0$) correspond to Andreev levels associated with the transition from a singlet ground-state to a doublet excited state. As discussed in the main text, increasing the field results in the Zeeman splitting of these levels. By carefully looking at Fig. 4a of ref. 10, a splitting may indeed be seen in the data although the split peak moving to higher energies disappears quickly into the edges of the superconducting gap. This seems even clearer in Fig. S12 of the same reference. On the other hand, no splitting is expected in the alternative scenario of a field-driven closure of the induced superconducting gap as confirmed by the numerical calculations in Fig. 4d of ref. 10. Thus, in the Andreev-level picture, the induced gap closure can be interpreted instead as the lowest-energy Zeeman-split level, $\zeta_{\uparrow}$, evolving linearly towards the Fermi energy.

In Fig. 4a of ref. 10, the ZBP appears to extend approximately from 40 to 70 mT. In the Andreev level picture, this corresponds to having $\zeta_{\uparrow} = 0$ at B= 55 mT. Given that $\zeta = 45\mu$eV for B=0, we estimate $|g| \approx 14$, a value pretty close to the electron g-factor in bulk InAs. From the energy width of the ZBP we estimate $w \approx 20\mu$eV. Based on these values, the expected field extension of the ZBP is $\Delta B \approx w/(|g|\mu_B) \approx 25$ mT, which is consistent with the field range estimated from the experimental data. Above 70 mT, the ZBP splits again. As opposed to an interpretation based on coupled MF edge states, this splitting can be readily understood as a result of the fact that increasing B stabilizes the $|\uparrow\rangle$ ground state leading to a sizable and growing excitation energy to the $|-\rangle$ state.

Based on the analysis above, a Zeeman-split Andreev level crossing the Fermi energy results in a ZBP with relatively limited extension, directly proportional to the ratio between its finite life-time broadening (w) and the g-factor. This cannot account for the large magnetic-field robustness of the ZBPs measured in hybrid devices based on InSb nanowires coupled to Nb-based superconducting electrodes. For instance, Mourik et al. [9] reported ZBPs extending over field ranges of several hundred mT, which is quite striking if one considers that g-factors in InSb NW are at least a few times larger than in InAs NWs. As we pointed out in the main text, however, the level repulsion between Andreev levels and the continuum of quasiparticle states can result in a significant stretching of the ZBP. In principle, a similar effect may be expected from other Andreev levels within the superconducting gap, as suggested by recent theoretical works [17, 18, 20, 21]. The data in the left panel of Fig. 3c (main text), provide an experimental demonstration of this effect as confirmed by the numerical simulations in the right panel of the same figure. Following the $|-\rangle \rightarrow |\uparrow\rangle$ quantum-phase transition, i.e. for $B > B_{QPT}$, the ζ peaks corresponding to the excitation from $|\uparrow\rangle$ to $|-\rangle$ are repelled by the quasiparticle states at the gap edge. As a result, the split peaks remain squeezed to zero-bias, thus stretching the ZBP up to a several hundred mT, i.e. well beyond the range expected from the w/g ratio. Having said so, the Andreev-level ZBPs observed in the present work exhibit a splitting at lower and, in cases like Fig. S7, higher fields. This characteristic is apparently absent in the ZBPs reported for InSb nanowires contacted by Nb-based superconducting electrodes [9, 13]. This dissimilarity seems to rule out an interpretation of those ZBPs within the simple picture of an Andreev-level pair at the Fermi energy.

B. Dependence of the Andreev-level ZBPs on the field angle.

The suppression of the ZBP when the external field is applied parallel to the spin-orbit field has been considered as one of the strongest indications in favor of a MF interpretation. We note that most of the reported experiments present their angular dependence data by fixing B at a position where the ZBP is visible, and then performing a field rotation at constant field magnitude. As mentioned in the main text, by carrying out our measurement of Andreev-level ZBPs in a similar way, we were able to recover the same qualitative features expected for MFs. As the angle dependence of Andreev-level ZBPs originates from g-factor anisotropy, however, a ZBP is also expected for $B \parallel B_{SO}$, yet at a different field magnitude (see Fig. S6). Thus, we argue that carrying out a full B-dependence also for $B \parallel B_{SO}$ (such as in Fig. S6a), and not simply a field rotation at constant field magnitude, is a useful control experiment to discriminate ZBPs due to MFs from those due to Andreev-levels.

C. Splitting of the ZBP and its magnetic-field induced oscillations.

Recently, a few experimental studies have reported either the splitting of the ZBP with increasing B [10], or a ZBP that appears and vanishes a few times over a large B sweep [12, 13]. These experimental observations have been interpreted as possible evidences of the coupling between MFs at the opposite edges of a nanowire segment with induced topological superconductivity. In the main text we have shown that the Andreev-level ZBP appears at $B = B_{QPT}$, where $\zeta_{\uparrow} = 0$ (Fig. 4a). Either above or below this field, a splitting of the ZBP is observed (Fig. 4a, Fig.S7). Therefore, in the simplest case of a single-level QD considered here, only one ZBP is expected, which is

DOI: 10.1038/NNANO.2013.267

centered around $B = B_{QPT}$. Still, due to the field-induced suppression of the superconducing gap, the split ζ peaks for $B > B_{QPT}$ converge back to zero-energy, an effect that can resemble like a re-emergence of a ZBP when B approaches to the critical field. (Fig. S7b). In case of a system with more than two Andreev levels in the superconducting gap, i.e., different than the small QD limit considered here, a ZBP may appear and disappear multiple times over a large field range due to different Andreev levels crossing the Fermi energy at different magnetic fields. This scenario has been discussed in recent theoretical works [17, 20].

References

[1] E. Vecino, A. Martín-Rodero and A. Levy Yeyati, *Phys. Rev. B* **68** 035105 (2003)
[2] A. Martín-Rodero and A. Levy Yeyati, *J. Phys.: Condens. Matter* **24** 385303 (2012).
[3] J. Bauer, A. Oguri and A. C. Hewson, J. Phys.: Condens. Matter **19**, 486211 (2007).
[4] T. Meng and S. Florens and P. Simon, Phys. Rev. B **79** 224521 (2009).
[5] J. D. Pillet, C. H. L. Quay, P. Morfin, C. Bena, A. Levy Yeyati and P. Joyez, *Nature Phys.* **6** 965 (2010).
[6] G.E. Blonder, M. Tinkham and T.M. Klapwijk, , Phys. Rev B **25**, 4515 (1982).
[7] R. M. Lutchyn, J. D. Sau and S. Das Sarma, *Phys. Rev. Lett.* **105** 077001 (2010).
[8] Y. Oreg, Refael, G. and von Oppen, F., *Phys. Rev. Lett.* **105** 177002 (2010).
[9] V. Mourik, K. Zuo, S. M. Frolov, S. R. Plissard, E. P. A. M. Bakkers and L. P. Kouwenhoven, *Science* **336** 1003 (2012).
[10] A. Das, Y. Ronen, Y. Most, Y. Oreg, M. Heiblum and H. Shtrikman, *Nature Phys.* **8** 887 (2012).
[11] M. T. Deng, C. L. Yu, G. Y. Huang, M. Larsson, P. Caroff and H. Q. Xu, *Nano Lett.* **12** 6414 (2012).
[12] A. D. K. Finck, D. J. van Harlingen, P. K. Mohseni, K. Jung and X. Li, *Phys. Rev. Lett.* **110** 126406 (2013).
[13] H. O. H. Churchill, V. Fatemi, K. Grove-Rasmussen, M. T. Deng, P. Caroff, H. Q. Xu and C. M. Marcus, arXiv:1304.2407v1 (2013).
[14] B. J. van Wees, P. de Vries, P. Magnée and T. M. Klapwijk, *Phys. Rev. Lett.* **69** 510 (1992).
[15] S. Hikami, A. I. Larkin and Y. Nagaoka, *Prog. Theor. Phys.* **63** 707 (1980).
[16] D. Goldhaber-Gordon, H. Shtrikman, D. Mahalu, D. Abusch-Magder, U. Meirav and M. A. Kastner, *Nature* **391** 156 (1998).
[17] E. Prada, P. San-José and R. Aguado, *Phys. Rev. B* **86** 180503(R) (2012).
[18] D. Rainis, J. Klinovaja and D. Loss, *Phys. Rev. B* **87** 024515 (2013).
[19] S. Das Sarma, J. D. Sau and T. D. Stanescu, *Phys. Rev. B* **86** 220506(R) (2012).
[20] J. Liu, A. C. Potter, K. T. Law and P. A. Lee, *Phys. Rev. Lett.* **109** 267002 (2012).
[21] G. Kells, D. Meidan and P. W. Brouwer, *Phys. Rev. B* **86** 100503(R) (2012).